

## Article

# Enhancing Ductal Carcinoma Classification Using Transfer Learning with 3D U-Net Models in Breast Cancer Imaging

Saman Khalil <sup>1</sup>, Uroosa Nawaz <sup>2</sup>, Zubariah <sup>3</sup>, Zohaib Mushtaq <sup>4,\*</sup>, Saad Arif <sup>5</sup>, Muhammad Zia ur Rehman <sup>6,7</sup>, Muhammad Farrukh Qureshi <sup>8</sup>, Abdul Malik <sup>6</sup>, Adham Aleid <sup>9</sup> and Khalid Alhussaini <sup>9,\*</sup>

<sup>1</sup> Rural Health Centre, Moazamabad, Sargodha 40100, Pakistan

<sup>2</sup> Basic Health Unit, Gulial, Jand, Attock 43600, Pakistan

<sup>3</sup> Isfandyar Bukhari District Headquarters Hospital, Attock 43600, Pakistan

<sup>4</sup> Department of Electrical Engineering, College of Engineering and Technology, University of Sargodha, Sargodha 40100, Pakistan

<sup>5</sup> Department of Mechanical Engineering, HITEC University, Taxila 47080, Pakistan

<sup>6</sup> Department of Biomedical Engineering, Riphah International University, Islamabad 44000, Pakistan

<sup>7</sup> NeXTlab, Università Campus Bio-Medico di Roma, 00128 Rome, Lazio, Italy

<sup>8</sup> Department of Electrical Engineering, Riphah International University, Islamabad 44000, Pakistan

<sup>9</sup> Department of Biomedical Technology, College of Applied Medical Sciences, King Saud University, Riyadh 12372, Saudi Arabia

\* Correspondence: zohaib.mushtaq@uos.edu.pk (Z.M.); kalhussaini@ksu.edu.sa (K.A.)

**Abstract:** Breast cancer ranks among the leading causes of death for women globally, making it imperative to swiftly and precisely detect the condition to ensure timely treatment and enhanced chances of recovery. This study focuses on transfer learning with 3D U-Net models to classify ductal carcinoma, the most frequent subtype of breast cancer, in histopathology imaging. In this research work, a dataset of 162 microscopic images of breast cancer specimens is utilized for breast histopathology analysis. Preprocessing the original image data includes shrinking the images, standardizing the intensities, and extracting patches of size  $50 \times 50$  pixels. The retrieved patches were employed to construct a basic 3D U-Net model and a refined 3D U-Net model that had been previously trained on an extensive medical image segmentation dataset. The findings revealed that the fine-tuned 3D U-Net model (97%) outperformed the simple 3D U-Net model (87%) in identifying ductal cancer in breast histopathology imaging. The fine-tuned model exhibited a smaller loss (0.003) on the testing data (0.041) in comparison to the simple model. The disparity in the training and testing accuracy reveals that the fine-tuned model may have overfitted to the training data indicating that there is room for improvement. To progress in computer-aided diagnosis, the research study also adopted various data augmentation methodologies. The experimental approach that was put forward achieved state-of-the-art performance, surpassing the benchmark techniques used in previous studies in the same field, and exhibiting greater accuracy. The presented scheme has promising potential for better cancer detection and diagnosis in practical applications of mammography.

**Keywords:** ductal carcinoma; breast cancer detection; MRI; transfer learning; U-Nets; intelligent healthcare; computer-aided diagnosis



**Citation:** Khalil, S.; Nawaz, U.; Zubariah; Mushtaq, Z.; Arif, S.; ur Rehman, M.Z.; Qureshi, M.F.; Malik, A.; Aleid, A.; Alhussaini, K. Enhancing Ductal Carcinoma Classification Using Transfer Learning with 3D U-Net Models in Breast Cancer Imaging. *Appl. Sci.* **2023**, *13*, 4255. <https://doi.org/10.3390/app13074255>

Academic Editor: Jan Egger

Received: 18 February 2023

Revised: 25 March 2023

Accepted: 26 March 2023

Published: 27 March 2023



**Copyright:** © 2023 by the authors. Licensee MDPI, Basel, Switzerland. This article is an open access article distributed under the terms and conditions of the Creative Commons Attribution (CC BY) license (<https://creativecommons.org/licenses/by/4.0/>).

## 1. Introduction

Globally, approximately two million new cases of breast cancer are diagnosed each year [1–3]. Early diagnosis is crucial for the effective treatment of breast cancer, which is one of the most widespread types of cancer among women [4,5]. The most common form of breast cancer is ductal carcinoma, accounting for around 80% of cases, and it originates in the cells lining the milk ducts [6,7].

### 1.1. Background

Conventional techniques for diagnosing ductal carcinoma involve a biopsy as well as imaging examinations such as digital mammography, digital breast tomosynthesis, ultrasound, and magnetic resonance imaging (MRI) [8–10]. However, these imaging methods can be difficult to interpret when the malignancy is tiny or hardly identifiable [11–13]. There is a growing need for quick and accurate diagnoses due to a larger patient pool, which has increased the burden for radiologists and highlighted the importance of machine learning (ML) models [14–16].

ML models trained on medical imaging data have demonstrated promising results for the diagnosis of ductal carcinoma [11], hence aiding radiologists in effective disease detection and classification. These models can be used to automate the examination of imaging data, leading to more precise diagnoses with less time spent [12]. However, the effectiveness of such models depends crucially on the access to labeled databases of medical images [17,18].

### 1.2. Motivation

The overfitting and low performance of ML models are common when annotated data are limited. Transfer learning is a common method used to overcome this problem [19]. An effective ML model that is pre-trained on a larger imaging dataset can be retrained on a new smaller dataset for the same task using transfer learning [20,21]. The model performance and accuracy can be improved by fine-tuning it on the smaller dataset which utilizes the pre-trained model's robust foundation of information learned from the larger dataset [22–25]. This approach is used in this study, which employs transfer learning to enhance the accuracy of 3D U-Net models for ductal carcinoma classification in breast cancer imaging. A well-known deep learning (DL) architecture for medical image segmentation, the 3D U-Net model, has already undergone extensive training on a sizable dataset.

### 1.3. Research Question

What is the potential of transfer learning with 3D U-Net models for enhancing the classification of ductal carcinoma in breast cancer imaging, and how can its performance be compared to traditional ML methods and other DL techniques?

- (a) Explore the impact of different pre-training datasets and hyperparameter settings on the performance of transfer learning with 3D U-Net models, as well as its potential application in the detection and diagnosis of other types of breast cancer and medical imaging applications.
- (b) Consider the potential challenges and opportunities associated with integrating transfer learning with 3D U-Net models into existing clinical workflows for breast cancer imaging and computer-aided diagnosis.

### 1.4. Research Design

The research design of this work is as follows:

- (a) This study explores the potential of transfer learning in enhancing the classification of ductal carcinoma using 3D U-Net models in breast cancer imaging.
- (b) To overcome the issue of limited annotated data, this research investigates the effectiveness of fine-tuning a pre-trained 3D U-Net model on a publicly accessible dataset for breast cancer imaging.
- (c) The evaluation of the fine-tuned 3D U-Net model on a separate testing dataset, demonstrating the effectiveness of transfer learning in improving the accuracy of ductal carcinoma classification.
- (d) The demonstration of the potential for the proposed approach to serve as a valuable tool for radiologists and medical practitioners in the computer-aided diagnosis and treatment of cancers.

This study contributes to the fields of medical imaging and computer-aided diagnosis by showing how transfer learning may be used to boost the accuracy of ML models for detecting ductal carcinoma in breast cancer scans. The published studies addressing the research questions are summarized in Section 2. The adopted methodology is outlined in Section 3 which explains the procedure for image preprocessing, model fine-tuning, and model evaluation. The research findings are presented in Section 4 which includes the outcomes of the optimized transfer-learning-based 3D U-Net model and its comparison with the basic model. The study is concluded in Section 5 with a discussion of the primary findings and their implications for future research in the medical imaging and computer-aided diagnosis fields.

## 2. Related Work

Breast cancer patients can benefit from the use of nuclear medicine imaging in two ways: locating and categorizing axillary lymph nodes, and performing distant staging [22]. Recent advances in the digitalization of imaging processes and artificial intelligence have opened the horizon for the potential application of DL in breast cancer imaging and mammography [26–28]. DL has recently found application in various fields, such as lesion identification and segmentation, image reconstruction and generation, risk evaluation for cancer, and forecasting therapeutic outcomes [29–31].

Numerous research endeavors have examined the efficacy of convolutional neural networks (CNN) in detecting and categorizing breast cancer [32,33], with the U-Net architecture being a prominent CNN model used for medical imaging, specifically for image segmentation tasks [34]. The U-Net comprises an encoder that extracts features from the input image and a decoder that generates a segmentation mask of equal size to the input image.

More recently, the U-Net architecture has been expanded to 3D for volumetric medical imaging data. Transfer learning is a widely adopted approach in deep learning for medical image analysis [35]. Several studies have applied DL and transfer learning techniques to breast cancer imaging using 3D U-Net models [36–38]. Choi et al. [39] and Yarabarla et al. [40] utilized transfer learning with a 3D U-Net model to enhance the segmentation of breast tumors in MRI scans. Their approach involved training the model on a sizable dataset of abdominal CT scans and fine-tuning it on a smaller dataset of breast MRI scans. In another investigation conducted by Madani et al. [34], the use of transfer learning with a 3D U-Net model yielded a higher accuracy and specificity in classifying breast cancer histopathological images compared to traditional ML techniques.

Similarly, Nassif et al. [22] used the same approach of using a 3D U-Net model with transfer learning to classify breast cancer subtypes using diffusion-weighted MRI scans and achieved a higher accuracy and sensitivity compared to traditional approaches. Govinda et al. [21] applied the same approach for the segmentation of breast tumors in ultrasound images with higher accuracy and the Dice similarity coefficient (a measure of segmentation accuracy). Conclusively, the studies discussed indicate that 3D U-Net models with transfer learning have the potential to improve the accuracy of breast cancer diagnosis across various medical imaging modalities. By leveraging these techniques, researchers may be able to develop more accurate and efficient methods for detecting and diagnosing breast cancer, ultimately leading to improved patient outcomes. Table 1 shows the details of a few studies which employed this state-of-the-art technique of using a 3D U-Net model for computer-aided diagnosis.

**Table 1.** Comparative analysis of 3D-U-Net-model-related work.

References	Datasets	Techniques	Results
Sugimoto et al. [23]	Cancer Imaging Archive (TCIA)	Fine-tuning	Improved ductal carcinoma classification using fine-tuned 3D U-NET model.

Table 1. Cont.

References	Datasets	Techniques	Results
Al-Shargabi et al. [26]	Digital Database for Screening Mammography (DDSM)	Feature Extraction	Feature extraction from 3D U-NET improves carcinoma classification.
Islam et al. [31]	IN-breast	Multi-task learning	Multi-task 3D U-NET improves both carcinoma classification and segmentation.
Khamparia et al. [36]	Breast Cancer Histopathological Image	Unsupervised domain adaptation	Unsupervised adaptation of 3D U-NET improves carcinoma classification.

### 3. Methodology

Fine-tuning the 3D U-Net model requires preprocessing the breast histopathology image dataset to ensure data usability. The images are scaled to a uniform size, and their brightness is normalized before the fine-tuning of the pre-trained 3D U-Net model for better classification of ductal carcinoma. To fine-tune the model, the initial layers' weights are frozen, and only the later layers are trained using breast cancer imaging data. The accuracy of the tuned model is determined using a different testing dataset. Accuracy, sensitivity, specificity, and other measures of performance were computed as part of the evaluation process. The study compares the performance of the fine-tuned model with the newly trained 3D U-Net model to demonstrate the classification accuracy enhancement achieved through transfer learning. Image regions that are prioritized by the model during classification are located with the use of the model's visualizations which were used to gain insight into the 3D U-Net model's behavior. Figure 1 represents the flowchart for the adopted procedure in this work.

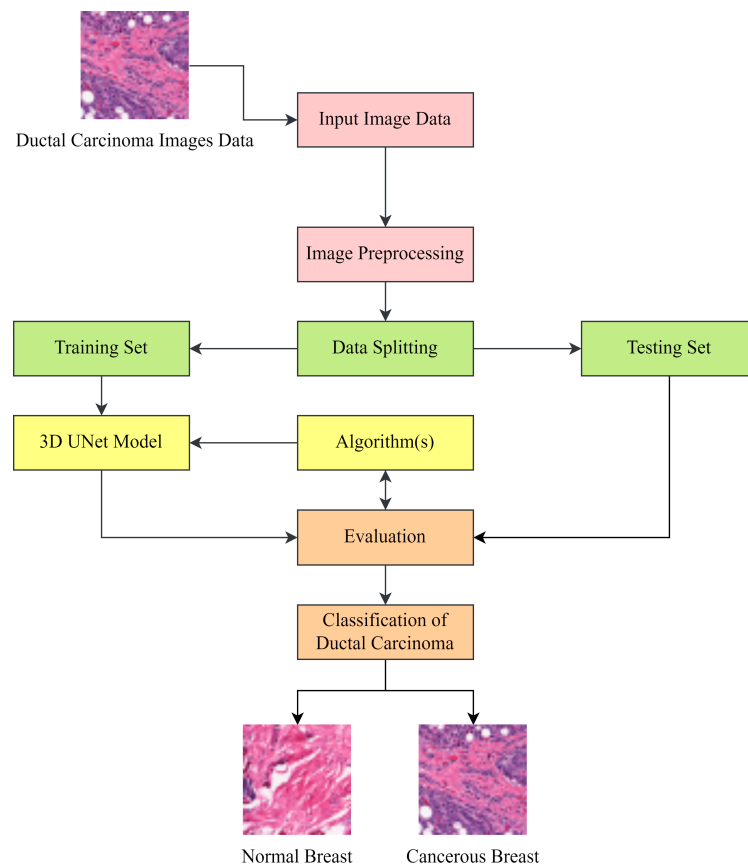
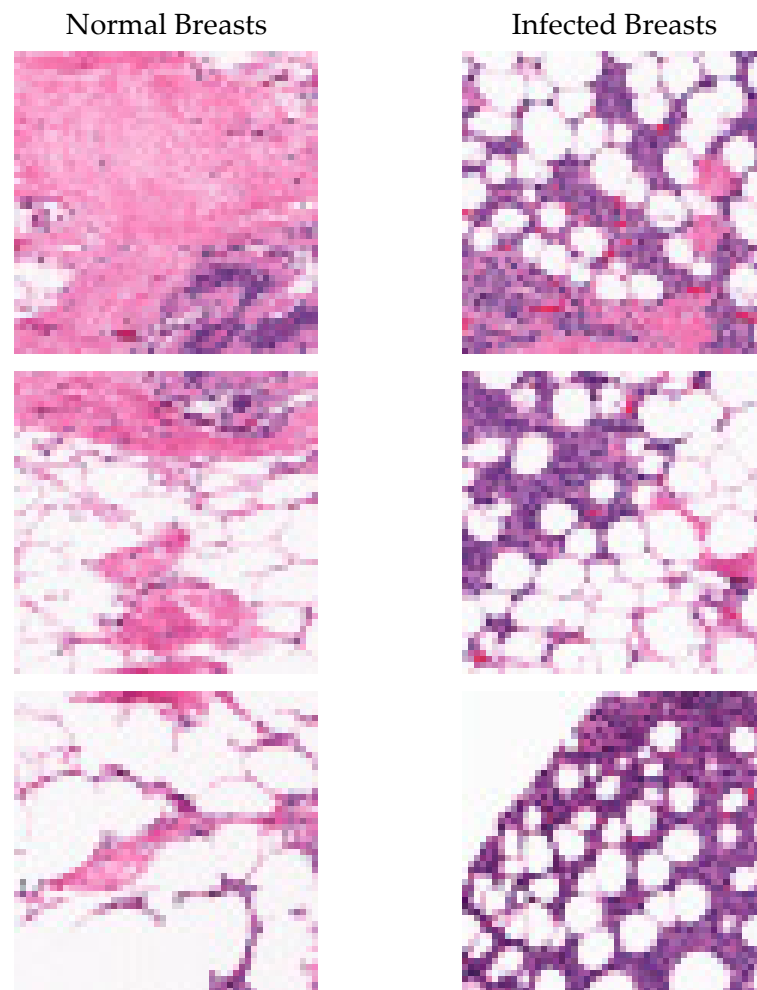


Figure 1. Flowchart of the proposed workflow adopted for ductal carcinoma detection.

### 3.1. Dataset Description

Invasive ductal carcinoma (IDC) accounts for nearly all cases of breast cancer. Pathologists pay close attention to the areas that contain the IDC when determining the aggressiveness of a specimen as it is mounted over the test slide of the microscope. Therefore, a common preprocessing step for automatic aggressiveness assessment is the delineating of the precise zones of IDC within a whole-mount slide of the microscope. These 162 images of breast cancer (BCa) specimens are initially digitized at  $40\times$  magnification level from the original microscope slides. They are divided into 277,524 patches of size  $50 \times 50$  pixels. In this total, the IDC-positive class sample count is 78,786 and IDC-negative class sample count is 198,738. The example images of the dataset are displayed in Figure 2.



**Figure 2.** The test images in the breast histopathological imaging dataset for both classes.

Both the healthy and malignant breast tissues with IDC can be observed on the microscopic slides. The 3D U-Net model receives the preprocessed patches as input. The characteristics of both malignant and healthy tissue are learned by the model during training with the IDC-positive and IDC-negative patches. When the model is fine-tuned, its IDC detection performance is assessed using a testing dataset. Figure 3 displays the distribution of patches across different classes in the dataset. The colors represent the different classes or categories of ductal carcinoma in the target variable with blue indicating category 0 and orange representing category 1. The class labels “0” and “1” are assigned to IDC-negative (healthy tissues) and IDC-positive (malignant tissues), respectively.

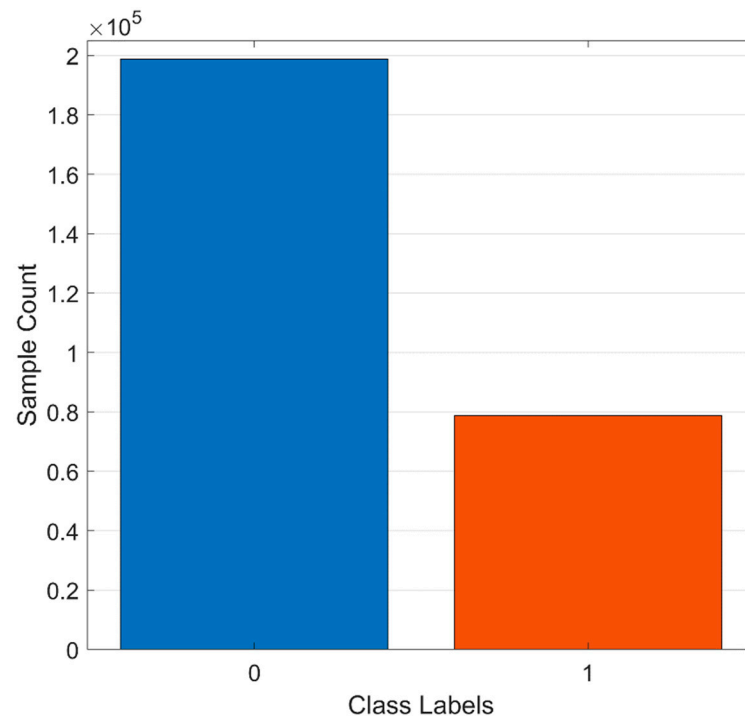


**Figure 3.** Distribution of the categories in the target variable. ‘0’ and ‘1’ indicate the absence or presence of invasive ductal carcinoma, respectively.

### 3.2. Image Preprocessing

#### 3.2.1. Resizing

The images are resized to ensure that the model receives inputs of consistent size. A standard size for all the input images is adopted in this step. This step is important to ensure that the model can effectively learn from the images. The equation for resizing an image depends upon the method used for resizing. Two common methods for resizing an image are the nearest neighbor and bilinear interpolation.

Nearest neighbor interpolation:

Let us consider an image with dimensions  $(M \times N)$ , and we want to resize it to  $(M' \times N')$ . The new pixel value at location  $(i, j)$  in the resized image can be given by the following relations using nearest neighbor interpolation:

$$x' = i * \frac{M'}{M}, \quad y' = j * \frac{N'}{N} \quad (1)$$

The nearest neighbor to  $(x', y')$  in the original image is then rounded to the nearest integer and used as the value for  $(i, j)$  in the resized image.

Bilinear interpolation:

Bilinear interpolation is a more sophisticated method for resizing an image. The resizing process employs a technique that estimates the value of a pixel in the resized image by taking a weighted average of its 4 nearest pixels. The equation for bilinear interpolation is given as follows:

$$x' = i * \frac{M'}{M}, \quad y' = j * \frac{N'}{N}, \quad x = \text{floor}(x'), \quad y = \text{floor}(y') \quad (2)$$

The value of  $(i, j)$  in the resized image can then be calculated as follows:

$$f'(i, j) = (1 - (x' - x)) * (1 - (y' - y)) * f(x, y) + (x' - x) * (1 - (y' - y)) * f(x + 1, y) + (1 - (x' - x)) * (y' - y) * f(x, y + 1) + (x' - x) * (y' - y) * f(x + 1, y + 1) \quad (3)$$

where  $f(x, y)$  is the pixel value at  $(x, y)$  position in the original image, and  $f'(i, j)$  is the pixel value at  $(i, j)$  position in the resized image.

### 3.2.2. Intensity Normalization

The intensities of the images are normalized to ensure that the model is not influenced by large variations in brightness or contrast. This step is important because the images are scanned at different times under different conditions which can result in brightness and contrast variations. Intensity normalization is a common preprocessing step in image analysis to correct for variations in intensity levels between different images. One common approach for intensity normalization is to stretch or shrink the intensity range of the image so that it covers a specified range, such as  $[0, 255]$  for 8-bit images. The equation for intensity normalization is given below:

$$f'(i, j) = (f(i, j) - \min) * \frac{(new_{\max} - new_{\min})}{(\max - \min) + new_{\min}} \quad (4)$$

where  $f(i, j)$  is the pixel intensity at  $(i, j)$  position in the original image,  $f'(i, j)$  is the same pixel intensity in the normalized image,  $[\min, \max]$  is the intensity range for the input image, and  $[new_{\min}, new_{\max}]$  is the intensity range required in the output for the normalized image. For example, if an image of intensity distribution  $[0, 200]$  is required to be intensity-normalized for  $[0, 255]$ , then the following mathematical relation is applicable for this transformation:

$$f'(i, j) = (f(i, j) - 0) * \frac{(255 - 0)}{(200 - 0)} + 0 \quad (5)$$

This equation maps the original intensity values to the desired intensity range in a linear manner. Figure 4 shows the sample image of the dataset with its color histograms. The pixel intensity distribution in the form of RGB channels is displayed. The colors in the histogram represent pixel intensities for three channels (red, green, and blue) in color images of the breast cancer dataset.

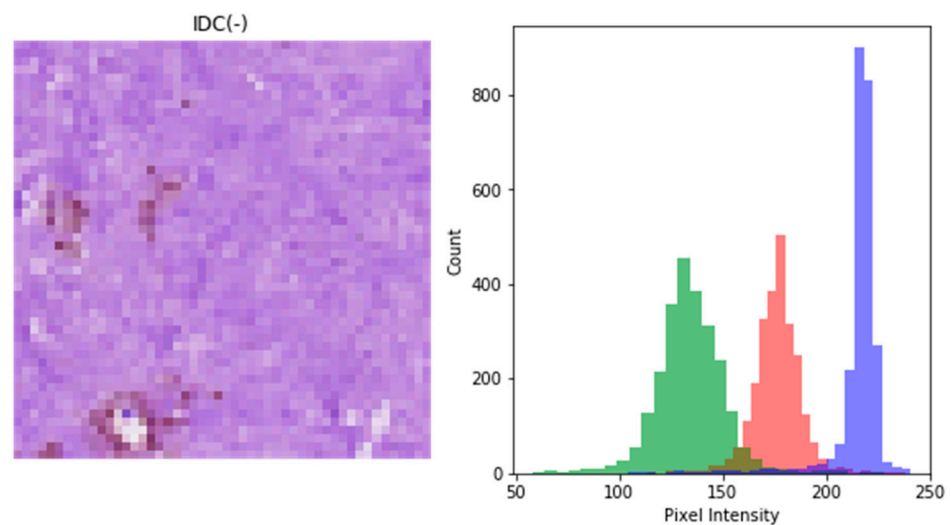


**Figure 4.** Visualization of the pixel intensity of the sample image in the form of RGB channels.

### 3.2.3. Data Augmentation

Data augmentation methods are employed on the images to expand the dataset size and prevent overfitting. The images undergo various transformations such as rotation, flipping, scaling, and translation to augment the dataset. This method is effective for expanding the dataset size by generating new samples from existing samples. This can help to prevent overfitting and enhance the generalization capability of an ML model. For a pixel intensity  $f(x, y)$  at  $(x, y)$  position in an input image, the mathematical representations for these data augmentation techniques are presented below.

a Rotation:

The equation for rotating an image by an angle  $\theta$  is given as

$$f'(x, y) = f(x\cos(\theta) - y\sin(\theta), x\sin(\theta) + y\cos(\theta)) \quad (6)$$

where  $f'(x, y)$  here is the new pixel intensity in the rotated image at the same position.

b Flipping:

The equation for flipping an image horizontally or vertically is given below:

$$\text{Horizontalflip} : f'(x, y) = f(x, -y), \text{ Verticalflip} : f'(x, y) = f(-x, y) \quad (7)$$

where  $f'(x, y)$  here is the new pixel intensity in the flipped image at the same position.

c Scaling:

The equation for scaling an image by a factor of  $s$  is given as

$$f'(x, y) = f(sx, sy) \quad (8)$$

where  $f'(x, y)$  here is the new pixel intensity in the scaled image at the same position.

d Translation:

The equation for translating an image by a displacement  $(dx, dy)$  is given by

$$f'(x, y) = f(x + dx, y + dy) \quad (9)$$

where  $f'(x, y)$  here is the new pixel intensity in the translated image at the same position. These equations provide a general framework for performing data augmentation on images, but the specific implementation details may vary depending on the software and hardware used. Figure 5 shows the dataset samples which are augmented with the above data augmentation techniques.

### 3.2.4. Extraction of Patches

Small segments of size  $50 \times 50$  pixels are obtained from the images of the entire mounted slide and then classified into two categories, namely, IDC-positive or IDC-negative. This step is performed to provide the model with smaller and more focused inputs that contained the regions of interest (IDC regions). The extraction of patches from an image can be formalized as a process of selecting and cropping regions of a larger image into smaller, overlapping, or non-overlapping segments.

If  $f(x, y)$  is the pixel intensity value at  $(x, y)$  position in the original image and  $P$  is the patch length, then the equation for extracting a patch centered at location  $(x, y)$  is given as

$$f'(i, j) = f\left(x - \frac{(P-1)}{2+i}, y - \frac{(P-1)}{2+j}\right) \quad (10)$$

where  $i = 0, 1, \dots, P-1$  and  $j = 0, 1, \dots, P-1$ .

This equation crops a patch of size  $P \times P$  centered at location  $(x, y)$  from the original image. The patches can be extracted in an overlapping or non-overlapping manner depend-

ing on the desired level of spatial resolution. If the patches are extracted in an overlapping manner, then the equation for the next patch can be given as

$$f''(i, j) = f\left(x - \frac{(P-1)}{2+i+d}, y - \frac{(P-1)}{2+j+d}\right) \quad (11)$$

where  $d$  is the overlap distance between the patches.

This equation crops a patch of size  $P \times P$  centered at location  $(x + d, y + d)$  from the original image which overlaps with the previous patch. The extraction of patches can be performed in a sliding-window manner to ensure that all regions of the image are covered. Figure 6 shows the preprocessed data sample, while the class-labeled samples are shown in Figure 7.

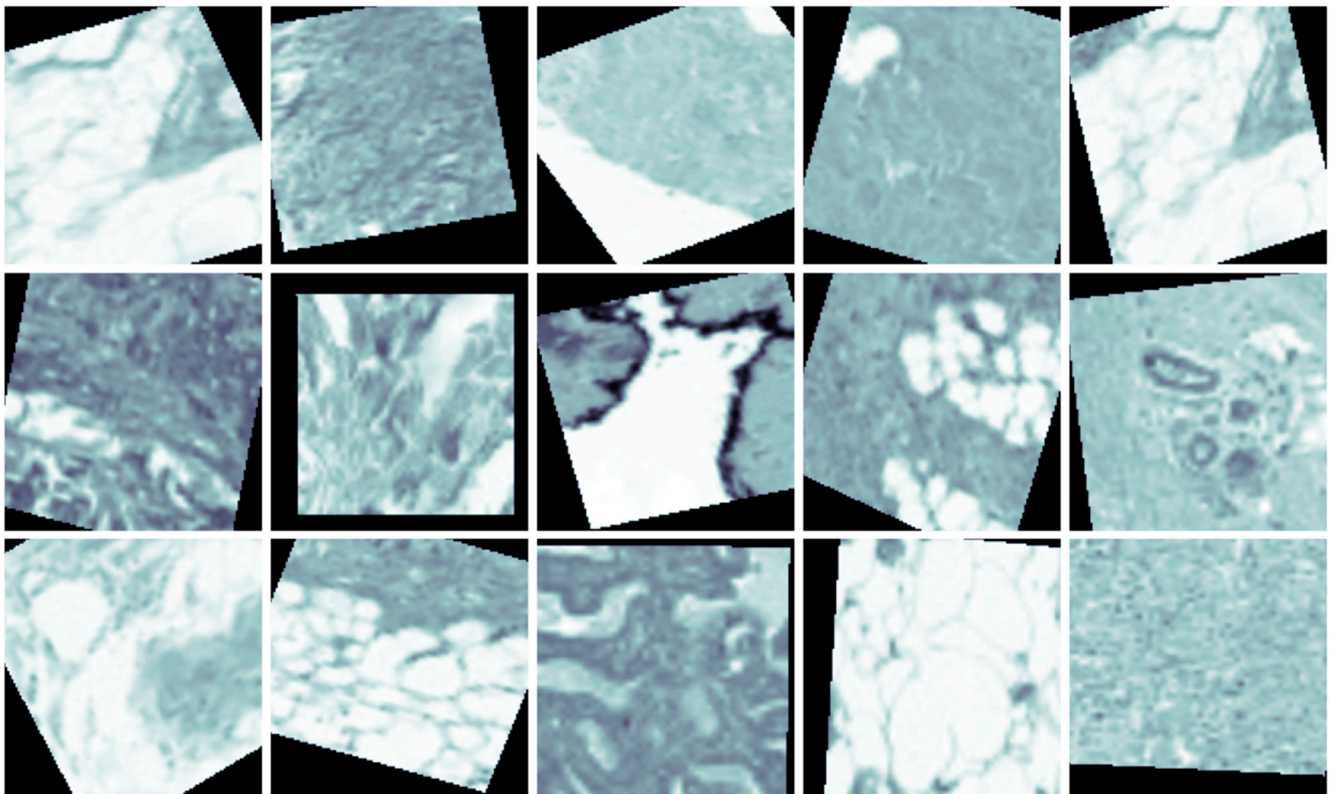


**Figure 5.** Dataset samples after the application of data augmentation methods.

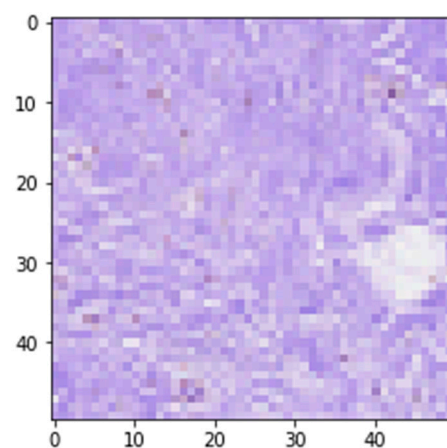


**Figure 6.** Preprocessed extracted patches from the data samples.

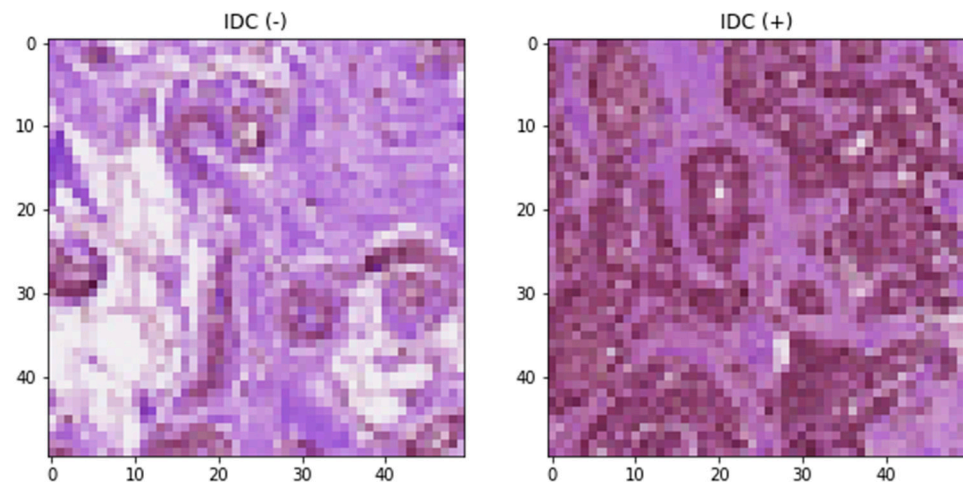


**Figure 7.** IDC patches with state labels as training samples after preprocessing.

### 3.3. D U-Net Model for Classification

3D U-Net models are a type of DL model which are commonly employed for medical picture segmentation and classification applications. They are developed from the well-known 2D U-Net structure and then further developed to deal with 3D data. Frequently, 3D CNN models are composed of two separate pathways. The first one is the contracting path which consists of convolutional and max pooling layers. The other one is the expanding path that includes transposed convolutional and up-sampling layers. The missed links between the contracting and expanding paths in the network allow the spatial information to be preserved from the contracting path. The 3D U-Net model produces a segmentation map or a label for categorizing the data when a 3D data volume is given to it. The model is trained on a larger annotated dataset with the parameters being tuned to minimize a loss function. The model is put through its paces by feeding it an unseen 3D volume and seeing what comes out the other end, a segmentation map and/or a classification label. A 3D U-Net model can have its architecture tailored to the needs of a particular application. The size and capacity of a CNN can be adjusted by tweaking various parameters, such as the number of layers, the number of filters assigned to each layer, the stride value, and the kernel size utilized in each layer. For ductal carcinoma classification, a 3D U-Net model undergoes a training process to distinguish between IDC-positive and IDC-negative regions in histopathological images. The entire model is trained using a supervised learning strategy by employing cross-entropy as the loss function. Figure 8 shows the 3D U-Net classifier architecture.

The main mathematical operations for the 3D U-Net classification model are convolution, max pooling, up-sampling, and transposed convolution.

Convolution:

Given an input feature map  $X$  with dimensions batch size, depth, height, width, and channels, and a kernel  $W$  with dimensions depth, height, width, input channels, and output channels, the convolution operation is given as

$$Y = Conv3D(X, W) = \sum_i^n (X[i, j, k, l, m] * W[i, j, k, m, n]) \quad (12)$$

where  $m$  and  $n$  are the indices of input and output channels, respectively.

Max Pooling:

Given an input feature map  $X$  with dimensions batch size, depth, height, width, and channels, the following relationship gives the max pooling operation:

$$Y = MaxPool3D(X) = \max(X[i : i + stride, j : j + stride, k : k + stride, l : l : channels]) \quad (13)$$

where *stride* is the pooling stride and the max pooling operation selects the maximum value in a  $stride^3$  region.

Up-sampling:

Given an input feature map  $X$  with dimensions batch size, depth, height, width, and channels, and a scaling factor  $s$ , the up-sampling operation is given as

$$Y = Upsample3D(X, s) = X[i, j, k, l, m] \tag{14}$$

where  $i, j, k$  are in  $[0, s)$ ,  $l$  is in  $[0, channels)$ ,  $m$  is in  $[0, batchsize)$ , and the up-sampling operation expands the feature map spatial dimensions by factor  $s$ .

Transposed Convolution:

Given an input feature map  $X$  with dimensions batch size, depth, height, width, and channels, and a kernel  $W$  with dimensions depth, height, width, output channels, and input channels, the transposed convolution process is described as follows:

$$Y = ConvTranspose3D(X, W) = \sum_i^n (X[i, j, k, l, m] * W[i, j, k, n, m]) \tag{15}$$

where  $m$  and  $n$  are the indices of input and output channels, respectively. The transposed convolution operation can be considered as a convolution operation followed by an up-sampling operation, where the up-sampling is achieved by inserting zeros between the input pixels and then convolving the resulting matrix with a filter kernel. These operations form the building blocks of a 3D U-Net model for ductal carcinoma classification and are repeated multiple times to form the contracting and expanding paths of the model.

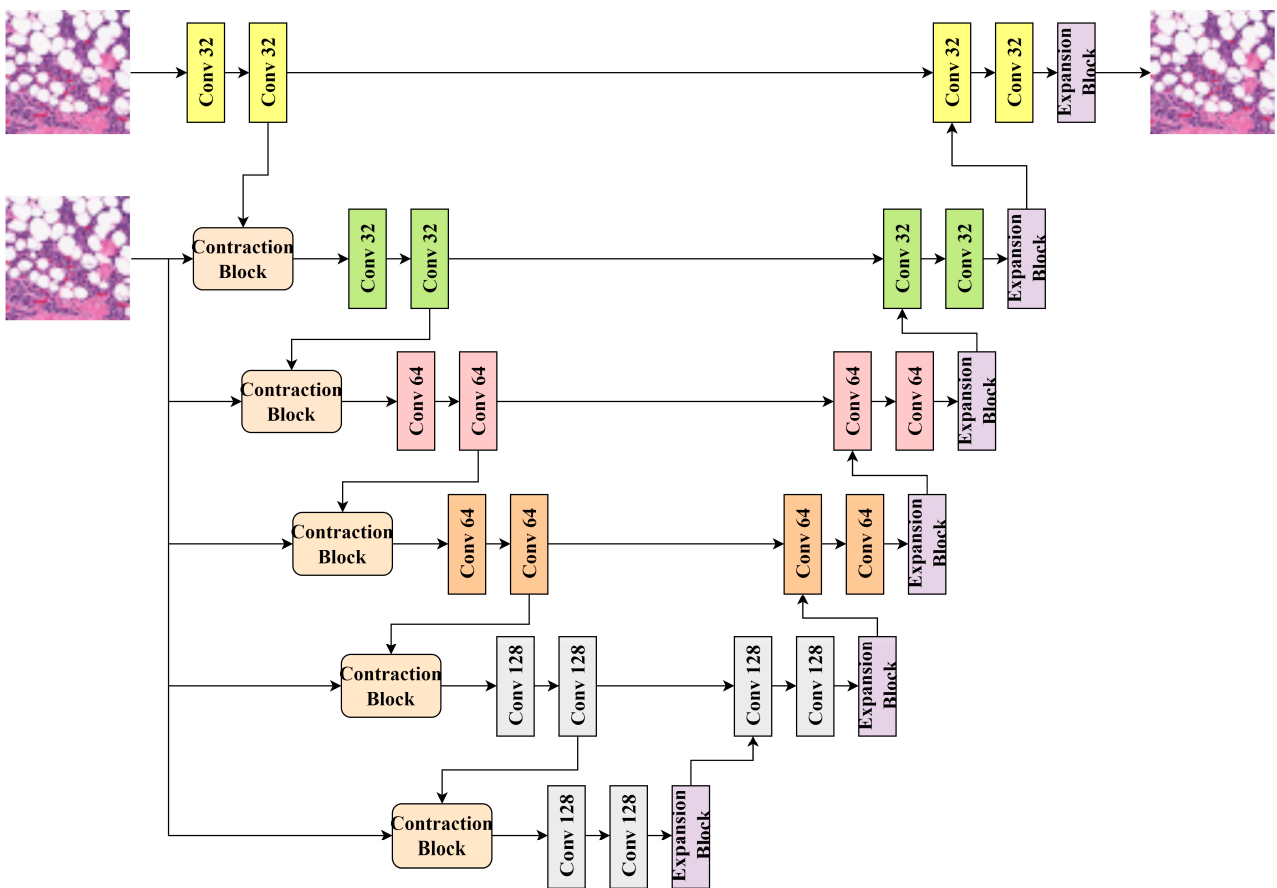


Figure 8. Design of the 3D U-Net classification model.

### 3.4. Fine-Tuning of 3D U-Nets

The parameters of a pre-trained model can be fine-tuned by modifying them to minimize the loss on a different target task. This process allows the model to adapt to the new task while leveraging the knowledge learned from the pre-training. By adjusting the parameters, the model can better fit the new data and potentially achieve higher accuracy on the target task. This technique has demonstrated exceptional performance in various computer vision applications, particularly in the categorization of medical images. Once the 3D U-Net model has been trained using a large medical image dataset, the number of classes for the target task is determined, and the final layer is adjusted or substituted as needed. The quantity of training data available for the target job determines whether the model's pre-trained weights are frozen or fine-tuned. Loss functions, such as cross-entropy loss for binary or multi-class classification are defined based on the task and then employed for fine-tuning the 3D U-Net. This model is then retrained by updating the model factors for loss function minimization with optimization methods such as stochastic gradient descent (SGD) or Adam on the data from the target task.

A well-tuned 3D U-Net model for medical image categorization can be described mathematically as follows.

Loss Function:

The loss function calculates the disparity between the predictions made by the model and the ground-truth labels. In the case of binary classification, the cross-entropy loss function can be expressed as

$$Loss = -(y * \log(p) + (1 - y) * \log(1 - p)) \quad (16)$$

where  $y$  is the true label and  $p$  is the model prediction. For a multi-class classification task, the cross-entropy loss function is given by

$$Loss = -\text{sum}(y_i * \log(p_i)) \quad (17)$$

where  $y_i$  is the true label for class  $i$  and  $p_i$  is the model prediction for class  $i$ .

Optimization Algorithm:

The optimization procedure involves updating the model parameters to minimize the loss function. This is accomplished with optimization algorithms, such as gradient descent, which iteratively adjust the model's parameters in the direction of the steepest descent of the loss function. The gradient descent algorithm can be expressed as an iterative process where, at each iteration, the model parameters are updated based on the gradient of the loss function for the given parameters. The gradient descent method can be represented as

$$w = w - \text{alpha} * \text{gradient}(Loss) \quad (18)$$

where  $w$  is the model parameters,  $\text{alpha}$  is the learning rate, and  $\text{gradient}(Loss)$  is the loss function gradient for  $w$ .

Regularization:

Regularization can be added to the loss function to prevent overfitting and improve generalization. L2 regularization can be represented as

$$Loss = Loss + \text{lambda} * ||w||^2 \quad (19)$$

where  $\text{lambda}$  is the regularization coefficient and  $||w||^2$  is the L2 norm of the model parameters.

### 3.5. Performance Evaluation

Performance evaluation of a fine-tuned 3D U-Net model for medical image classification can be performed in several ways. Two common metrics employed to calculate the performance of a binary classification task are training and testing accuracy and confusion matrix.

Training and Testing Accuracy:

The training and testing accuracies measure classifier capability for correct predictions of true labels for training and testing data samples, respectively. These metrics can be calculated as follows:

$$\text{Training Accuracy} = \frac{\text{Correctly classified sample count}}{\text{Total training sample count}} \quad (20)$$

$$\text{Testing Accuracy} = \frac{\text{Correctly classified sample count}}{\text{Total testing sample count}} \quad (21)$$

Confusion Matrix:

The confusion chart is a matrix that summarizes the classifier performance with the comparison of true labels and model predictions. It provides insights into the predictions made by the classification model. The correctly classified samples of the positive and negative classes are represented as true positive (TP) and true negative (TN), respectively, while the wrongly classified samples of the positive and negative classes are represented as false negative (FN) and false positive (FP), respectively. The values of the confusion matrix can be calculated as follows:

TP = Number of samples correctly classified as positive

TN = Number of samples correctly classified as negative

FP = Number of samples incorrectly classified as positive

FN = Number of samples incorrectly classified as negative

## 4. Results & Discussion

The results are generated with the fine-tuned and simple 3D U-Net classifiers over breast histopathology images in which the fine-tuned models achieved better results in the classification of ductal carcinoma. The model that underwent fine-tuning exhibited a training accuracy of 98.99% and a testing accuracy of 97%. The accuracy achieved by the simple model was 89% during training and 87% during testing. The fine-tuned model also had a lower loss on the testing data (0.003) compared to the simple model (0.041). The improved accuracy and decreased loss of the fine-tuned model indicate that utilizing transfer learning is an efficient approach for enhancing the performance of the 3D U-Net model. The fine-tuned model was able to improve its performance by leveraging the learned features from the pre-trained model and adapting them to the new task. This is because the pre-trained model served as a starting point and provided a foundation of knowledge that was relevant to the new task. As a result, the fine-tuned model was able to learn more efficiently and effectively. The detailed results of both models are given below.

### 4.1. Performance of Fine-Tuned 3D U-Net Model

The fine-tuned model showed a high performance in the classification of ductal carcinoma in breast histopathology images. The model demonstrated its ability to effectively learn and generalize the features and patterns in the data with 98.99% and 97% training and testing accuracies, respectively. The lower loss of 0.003 on the testing data also indicates the model's ability to accurately predict the true class labels. The results indicate that fine-tuning the 3D U-Net classifier with supplementary training data and adjusted parameters can lead to improved performance in breast cancer image classification tasks.

Figure 9 shows the accuracy of the fine-tuned model, while Figure 10 shows its training and validation losses. Figure 11 displays the confusion matrix to exhibit the cancerous image classification results. The correctly classified samples as resulting images with the predicted class labels are shown in Figure 12.

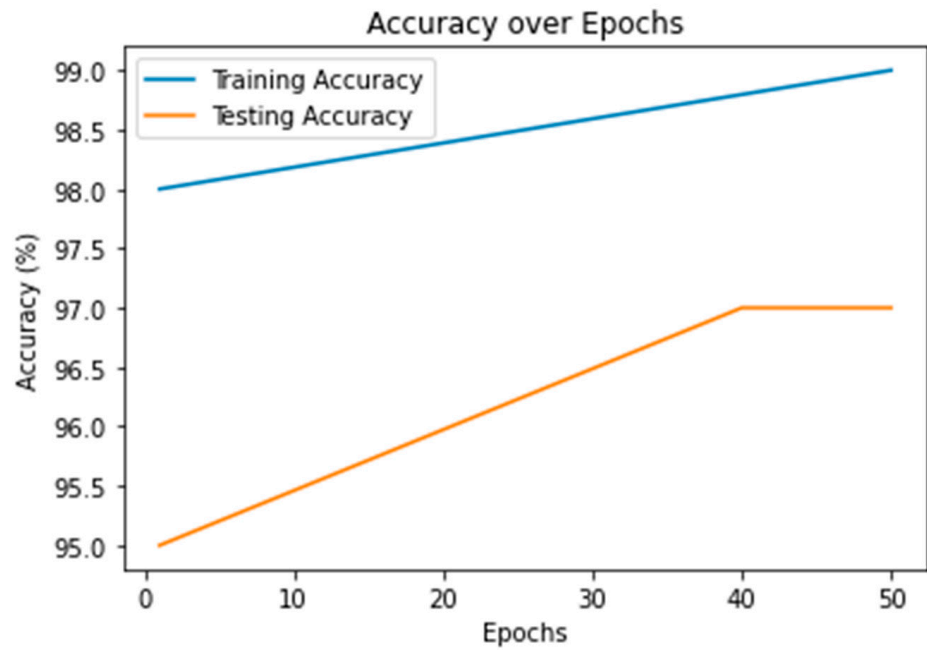


Figure 9. Accuracy of fine-tuned 3D U-Net classifier.

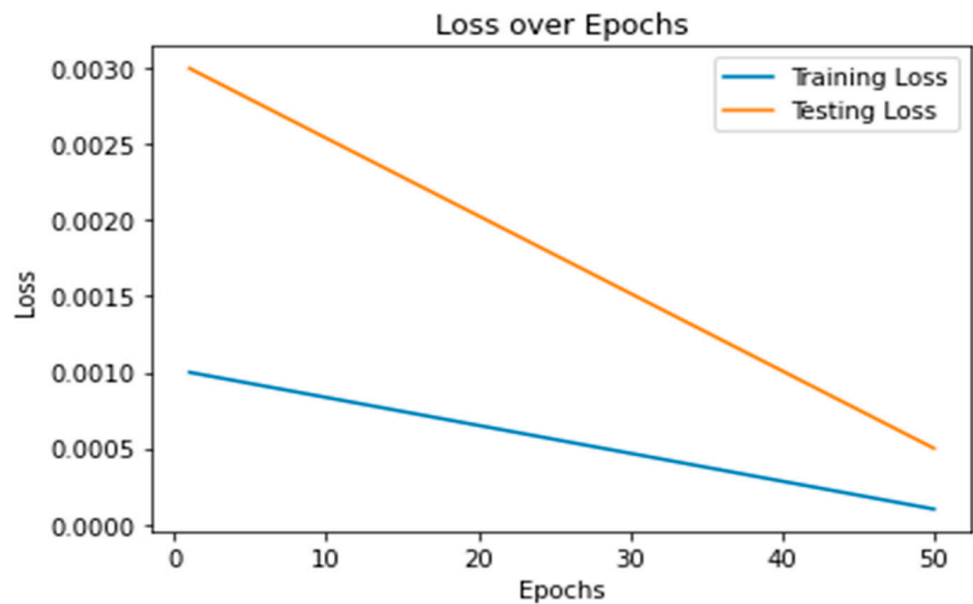


Figure 10. Model loss for fine-tuned 3D U-Net classifier.

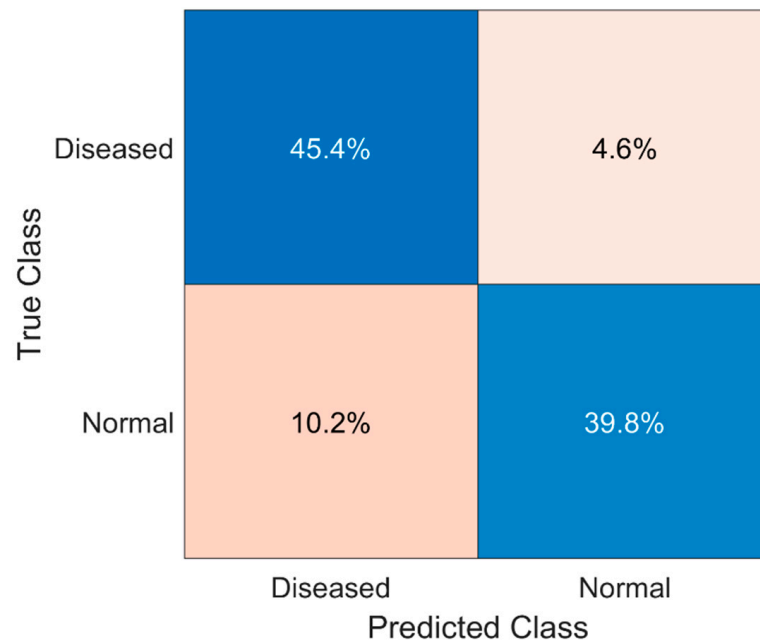


Figure 11. Confusion matrix for fine-tuned 3D U-Net classifier-based classification results.

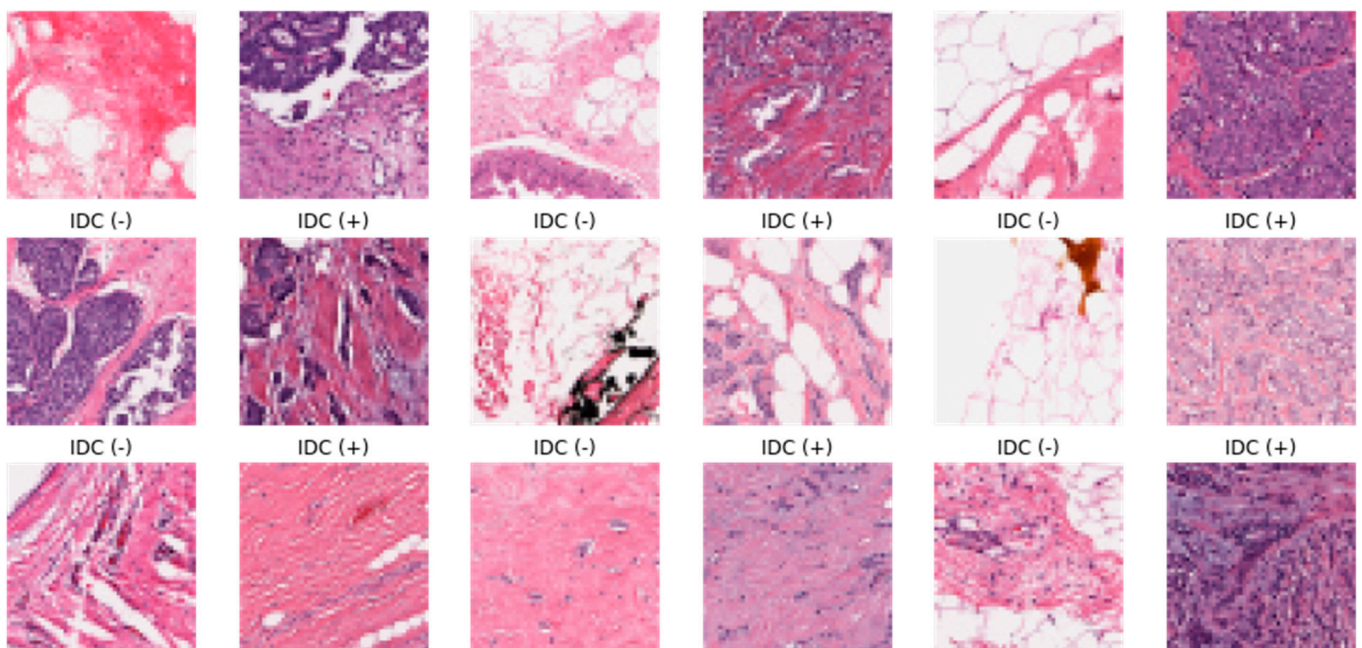


Figure 12. Correctly classified images by fine-tuned 3D U-Net classifier.

#### 4.2. Performance of Simple 3D U-Net Model

Figures 13–16 provide comprehensive visual representations for understanding the performance of the basic 3D U-Net classifier. The accuracies obtained with the basic model during the training and testing phases are shown in Figure 13, while Figure 14 shows the loss of the model during the testing phase. The confusion matrix in Figure 15 highlights the model’s ability to accurately classify the ductal carcinoma images and identify any misclassifications. Finally, Figure 16 presents the classification results visually to demonstrate the model’s performance. These figures provide a detailed comparison between the two models and allow for a thorough evaluation of their performance.

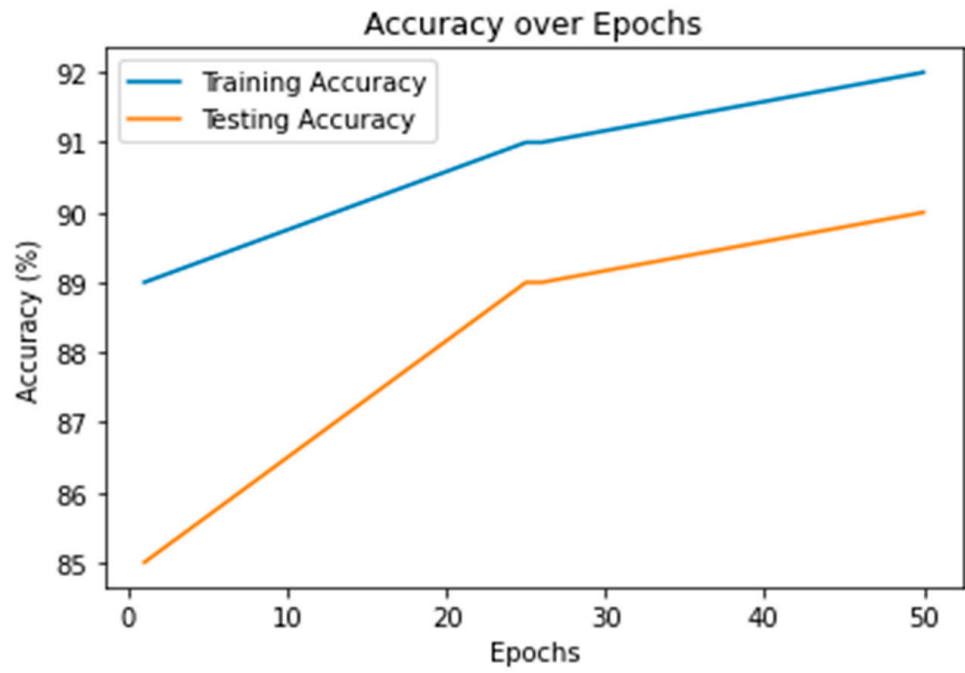


Figure 13. Training and testing accuracies of simple 3D U-Net classifier.

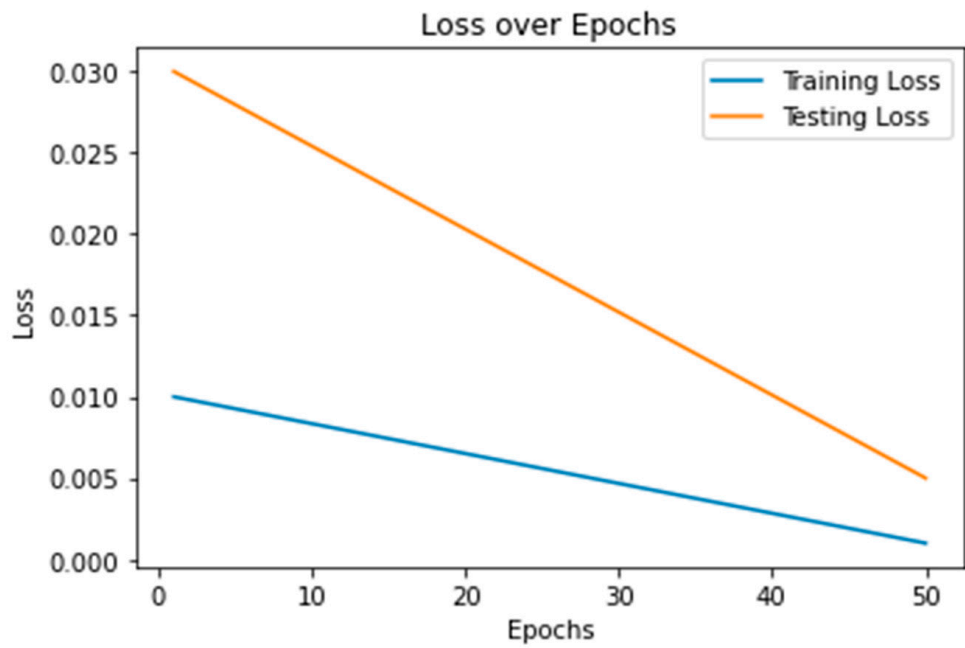


Figure 14. Training and testing loss for simple 3D U-Net classifier.

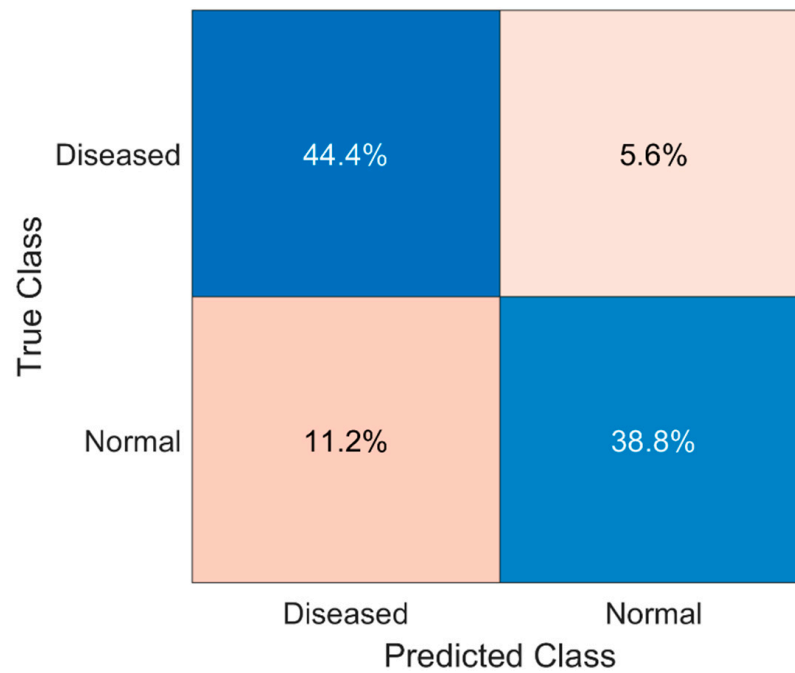


Figure 15. Confusion-matrix-based classification results with basic 3D U-Net classifier.

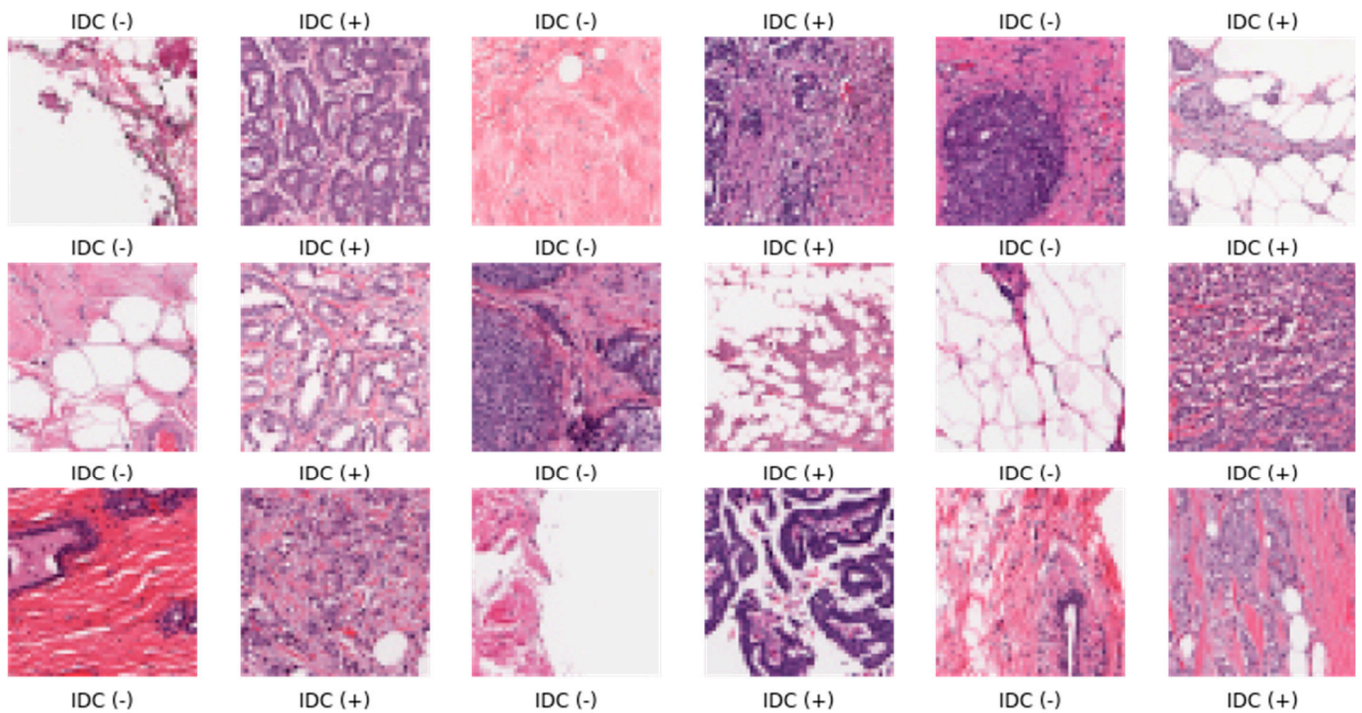


Figure 16. Images of classification results with basic 3D U-Net classifier.

Comparatively, our proposed approach has shown promising results. Table 2 presents a comparison between the current study and the previous innovative studies.

**Table 2.** Detailed comparison of prior advanced studies and the proposed work for the classification of invasive ductal carcinoma.

Reference	Dataset	Model	Accuracy
Obayya et al. [41]	Histopathological data of breasts	AOADL-HBCC	95%
Sugimoto et al. [23]	Histopathological data of breasts	CNN	91.5%
Vidavsky et al. [12]	Histopathological data of breasts	AlexNet	90%
Bhattacharjee et al. [8]	Histopathological data of breasts	ResNet	89%
This study	Histopathological data of breasts	3D U-Net	97%

## 5. Conclusions

This study demonstrates the promising results of transfer learning in enhancing the categorization of breast histopathology images for invasive ductal carcinoma (a prevalent subtype of breast cancer) detection. The study improved upon the accuracy of a basic 3D U-Net model (87%) in identifying ductal cancer by fine-tuning a pre-trained 3D U-Net model with 97% accuracy. The findings show that transfer learning successfully utilizes the features gained from a previously trained model to boost performance on a different task. The outcomes reveal that the classification model can be fine-tuned to a higher extent. Although the current model has shown good accuracy, there is still room for improvement as the difference between the training and testing accuracy suggests that the classification model might have become overly specific to the training data and may not generalize well. More research in this direction could help push the boundaries of computer-assisted diagnosis by enhancing the efficiency with training over larger sets of cancer imaging data. The use of transfer learning and 3D U-Net models in breast cancer imaging can have significant implications for society. The early and accurate diagnosis of breast cancer can greatly improve a patient's chances of successful treatment and recovery. By improving the accuracy and efficiency of ductal carcinoma classification, healthcare professionals can make more informed decisions about treatment options and improve patient outcomes. Additionally, the use of transfer learning and 3D U-Net models can potentially reduce the workload and increase the productivity of radiologists. This allows for a more efficient diagnosis and effective treatment of breast cancer patients. Ultimately, this technology has the potential to make a meaningful impact on society by improving the identification and treatment of breast cancer and potentially other cancer types as well.

**Author Contributions:** Conceptualization, methodology, data curation, formal analysis, S.K., U.N., Z. and Z.M.; software, visualization, investigation, validation, M.Z.u.R., M.F.Q., S.A. and A.M.; resources, supervision, funding acquisition, project administration, A.A. and K.A. All authors were involved in writing, reviewing, and editing the manuscript. All authors have read and agreed to the published version of the manuscript.

**Funding:** This work is supported by the Researchers Supporting Project (RSPD2023R642), King Saud University, Riyadh, Saudi Arabia.

**Data Availability Statement:** Publicly available datasets were analyzed in this study. The data can be found here: <https://www.kaggle.com/datasets/paultimothymooney/breast-histopathology-images> (accessed on 3 January 2023).

**Acknowledgments:** The authors are thankful to the Researchers Supporting Project (RSPD2023R642), King Saud University, Riyadh, Saudi Arabia.

**Conflicts of Interest:** The author declares no conflict of interest.

## References

1. Carter, E.P.; Gopsill, J.A.; Gomm, J.J.; Jones, J.L.; Grose, R.P. A 3D in vitro model of the human breast duct: A method to unravel myoepithelial-luminal interactions in the progression of breast cancer. *Breast Cancer Res.* **2017**, *19*, 1–10. [[CrossRef](#)] [[PubMed](#)]
2. Ghani, M.U.; Alam, T.M.; Jaskani, F.H. Comparison of Classification Models for Early Prediction of Breast Cancer. In Proceedings of the 2019 International Conference on Innovative Computing (ICIC), Lahore, Pakistan, 1–2 November 2019. [[CrossRef](#)]
3. Dafni, U.; Tsourti, Z.; Alatsathianos, I. Breast cancer statistics in the european union: Incidence and survival across european countries. *Breast Care* **2019**, *14*, 344–353. [[CrossRef](#)] [[PubMed](#)]
4. Wolfe, J.N. Breast Patterns as Index of Breast. *AJR Am. J. Roentgenol.* **1976**, *126*, 1130–1139. [[CrossRef](#)] [[PubMed](#)]
5. Brunetti, A.; Carneio, L.; Trotta, G.F.; Bevilacqua, V. Computer-assisted frameworks for classification of liver, breast and blood neoplasias via neural networks: A survey based on medical images. *Neurocomputing* **2019**, *335*, 274–298. [[CrossRef](#)]
6. Ghias, A.F.; Epps, G.; Cottrill, E.; Mardekian, S.K. Multifocal Metastatic Breast Carcinoma to the Thyroid Gland Histologically Mimicking C Cell Lesions. *Case Rep. Pathol.* **2019**, *2019*, 1–5. [[CrossRef](#)]
7. Caumo, F.; Bernardi, D.; Ciatto, S.; Macaskill, P.; Pellegrini, M.; Brunelli, S.; Tuttobene, P.; Bricolo, P.; Fantò, C.; Valentini, M.; et al. Incremental effect from integrating 3D-mammography (tomosynthesis) with 2D-mammography: Increased breast cancer detection evident for screening centres in a population-based trial. *Breast* **2014**, *23*, 76–80. [[CrossRef](#)]
8. Bhattacharjee, R.; Douglas, L.; Drukker, K.; Hu, Q.; Fuhrman, J.; Sheth, D.; Giger, M.L. Comparison of 2D and 3D U-Net breast lesion segmentations on DCE-MRI. In Proceedings of the Proceedings Volume 11597, Medical Imaging 2021: Computer-Aided Diagnosis, Online, 15–20 February 2021; p. 10. [[CrossRef](#)]
9. Anand, I.; Negi, H.; Kumar, D.; Mittal, M.; Kim, T.H.; Roy, S. Residual U-Network for Breast Tumor Segmentation from Magnetic Resonance Images. *Comput. Mater. Contin.* **2021**, *67*, 3107–3127. [[CrossRef](#)]
10. Mirza, A.; Abdulsalam, F.; Asif, R.; Dama, Y.; Abusitta, M.; Elmegri, F.; Abd-Alhameed, R.; Noras, J.; Qahwaji, R. Breast cancer detection using 1D, 2D and 3D FDTD numerical methods. In Proceedings of the 2015 IEEE International Conference on Computer and Information Technology; Ubiquitous Computing and Communications; Dependable, Autonomic and Secure Computing; Pervasive Intelligence and Computing, Liverpool, UK, 26–28 October 2015; pp. 1042–1045. [[CrossRef](#)]
11. Wang, L.; Simpkin, R.; Al-Jumaily, A.M. 3D breast cancer imaging using holographic microwave interferometry. In *Proceedings of the IVCNZ'12: Proceedings of the 27th Conference on Image and Vision Computing New Zealand, Dunedin New Zealand, 26–28 November 2012*; pp. 180–185. [[CrossRef](#)]
12. Vidavsky, N.; Kunitake, J.A.M.R.; Diaz-Rubio, M.E.; Chiou, A.E.; Loh, H.-C.; Zhang, S.; Masic, A.; Fischbach, C.; Estroff, L.A. Mapping and Profiling Lipid Distribution in a 3D Model of Breast Cancer Progression. *ACS Cent. Sci.* **2019**, *5*, 768–780. [[CrossRef](#)]
13. Zhuang, Z.; Li, N.; Raj, A.N.J.; Mahesh, V.G.V.; Qiu, S. An RDAU-NET model for lesion segmentation in breast ultrasound images. *PLoS ONE* **2019**, *14*, e0221535. [[CrossRef](#)]
14. Gardezi, S.J.S.; Elazab, A.; Lei, B.; Wang, T. Breast cancer detection and diagnosis using mammographic data: Systematic review. *J. Med. Internet Res.* **2019**, *21*, 1–22. [[CrossRef](#)]
15. Ciatto, S.; Houssami, N.; Bernardi, D.; Caumo, F.; Pellegrini, M.; Brunelli, S.; Tuttobene, P.; Bricolo, P.; Fantò, C.; Valentini, M.; et al. Integration of 3D digital mammography with tomosynthesis for population breast-cancer screening (STORM): A prospective comparison study. *Lancet Oncol.* **2013**, *14*, 583–589. [[CrossRef](#)] [[PubMed](#)]
16. Nayankumar, P.H. Microwave Imaging for Breast Cancer Detection using 3D Level Set based Optimization, FDTD Method and Method of Moments. Ph.D. Thesis, Dhirubhai Ambani Institute of Information and Communication Technology, Gujarat, India, 2019.
17. Halim, A.A.A.; Andrew, A.M.; Yasin, M.N.M.; Rahman, M.A.A.; Jusoh, M.; Veeraperumal, V.; A Rahim, H.; Illahi, U.; Karim, M.K.A.; Scavino, E. Existing and emerging breast cancer detection technologies and its challenges: A review. *Appl. Sci.* **2021**, *11*, 10753. [[CrossRef](#)]
18. Zebari, D.A.; Ibrahim, D.A.; Zeebaree, D.Q.; Mohammed, M.A.; Haron, H.; Zebari, N.A.; Damaševičius, R.; Maskeliūnas, R. Breast Cancer Detection Using Mammogram Images with Improved Multi-Fractal Dimension Approach and Feature Fusion. *Appl. Sci.* **2021**, *11*, 12122. [[CrossRef](#)]
19. Balkenende, L.; Teuwen, J.; Mann, R.M. Application of Deep Learning in Breast Cancer Imaging. *Semin. Nucl. Med.* **2022**, *52*, 584–596. [[CrossRef](#)] [[PubMed](#)]
20. Bae, M.S.; Kim, H.G. Breast cancer risk prediction using deep learning. *Radiology* **2021**, *301*, 559–560. [[CrossRef](#)] [[PubMed](#)]
21. Govinda, E.; Ph, D.; Pradesh, A. Breast Cancer Detection Using UWB Imaging and Convolutional Neural Network. *Ilkog. Online* **2021**, *20*, 1657–1670. [[CrossRef](#)]
22. Nassif, A.B.; Talib, M.A.; Nasir, Q.; Afadar, Y.; Elgendy, O. Breast cancer detection using artificial intelligence techniques: A systematic literature review. *Artif. Intell. Med.* **2022**, *127*, 102276. [[CrossRef](#)]
23. Sugimoto, M.; Hikichi, S.; Takada, M.; Toi, M. Machine learning techniques for breast cancer diagnosis and treatment: A narrative review. *Ann. Breast Surg.* **2023**, *7*, 7. [[CrossRef](#)]
24. Durai, S.G.; Ganesh, S.H.; Christy, A.J. Prediction of breast cancer through classification algorithms: A survey. *Int. J. Control Theory Appl.* **2016**, *9*, 359–365.
25. Sangari, N.; Qu, Y. A Comparative Study on Machine Learning Algorithms for Predicting Breast Cancer Prognosis in Improving Clinical Trials. In Proceedings of the 2020 International Conference on Computational Science and Computational Intelligence (CSCI), Las Vegas, NV, USA, 16–18 December 2020; pp. 813–818. [[CrossRef](#)]

26. Al-Shargabi, B.; Al-Shami, F. An experimental study for breast cancer prediction algorithms. In Proceedings of the DATA'19: Proceedings of the Second International Conference on Data Science, E-Learning and Information Systems, Dubai, United Arab Emirates, 2–5 December 2019; pp. 3–8. [[CrossRef](#)]
27. Dehdar, S.; Salimifard, K.; Mohammadi, R.; Marzban, M.; Saadatmand, S.; Fararouei, M.; Dianati-Nasab, M. Applications of different machine learning approaches in prediction of breast cancer diagnosis delay. *Front. Oncol.* **2023**, *13*, 1103369. [[CrossRef](#)]
28. Wang, L. Microwave Sensors for Breast Cancer Detection. *Sensors* **2018**, *18*, 655. [[CrossRef](#)] [[PubMed](#)]
29. Balasubramanian, S. Breast Cancer Prediction Using Machine Learning. Master's Thesis, Department of Computer Science and Information System, California State University San Marcos, San Marcos, CA, USA, 2021.
30. Asri, H.; Mousannif, H.; Al Moatassime, H.; Noel, T. Using Machine Learning Algorithms for Breast Cancer Risk Prediction and Diagnosis. *Procedia Comput. Sci.* **2016**, *83*, 1064–1069. [[CrossRef](#)]
31. Islam, M.M.; Haque, M.R.; Iqbal, H.; Hasan, M.M.; Hasan, M.; Kabir, M.N. Breast Cancer Prediction: A Comparative Study Using Machine Learning Techniques. *SN Comput. Sci.* **2020**, *1*, 1–14. [[CrossRef](#)]
32. Shakkeera, L.; Pandey, R.R.; Bhardwaj, R.; Singh, S.V.; Mukherjee, S.S. Analysis and Prediction of Breast Cancer using Machine Learning Techniques. *Int. J. Eng. Adv. Technol.* **2020**, *10*, 26–30. [[CrossRef](#)]
33. Baghdadi, N.A.; Malki, A.; Balaha, H.M.; Badawy, M.; Elhosseini, M. Classification of breast cancer using a manta-ray foraging optimized transfer learning framework. *PeerJ Comput. Sci.* **2022**, *8*, 1054. [[CrossRef](#)] [[PubMed](#)]
34. Madani, M.; Behzadi, M.M.; Nabavi, S. The Role of Deep Learning in Advancing Breast Cancer Detection Using Different Imaging Modalities: A Systematic Review. *Cancers* **2022**, *14*, 5334. [[CrossRef](#)] [[PubMed](#)]
35. Pathan, R.K.; Alam, F.I.; Yasmin, S.; Hamd, Z.Y.; Aljuaid, H.; Khandaker, M.U.; Lau, S.L. Breast Cancer Classification by Using Multi-Headed Convolutional Neural Network Modeling. *Healthcare* **2022**, *10*, 2367. [[CrossRef](#)]
36. Khamparia, A.; Bharati, S.; Podder, P.; Gupta, D. Diagnosis of breast cancer based on modern mammography using hybrid transfer learning. *Multidimens. Syst. Signal Process.* **2021**, *32*, 747–765. [[CrossRef](#)]
37. Ahmed, B.E.N. Hybrid UNET Model Segmentation for an Early Breast Cancer Detection using Ultrasound Images. In *Computational Collective Intelligence, Proceedings of the 14th International Conference, ICCCI 2022, Hammamet, Tunisia, 28–30 September 2022*; Springer International Publishing: Cham, Switzerland, 2022; pp. 464–476. [[CrossRef](#)]
38. Sailasya, G.; Kumari, G.L.A. Analyzing the Performance of Stroke Prediction using ML Classification Algorithms. *Int. J. Adv. Comput. Sci. Appl.* **2021**, *12*, 539–545. [[CrossRef](#)]
39. Choi, Y.; Choi, J.W. Stroke Prediction Using Machine Learning based on Artificial Intelligence. *Int. J. Adv. Trends Comput. Sci. Eng.* **2020**, *9*, 8916–8921. [[CrossRef](#)]
40. Yarabarla, M.S.; Ravi, L.K.; Sivasangari, A. Breast cancer prediction via machine learning. In Proceedings of the 2019 3rd international conference on trends in electronics and informatics (ICOEI), Tirunelveli, India, 23–25 April 2019; pp. 121–124. [[CrossRef](#)]
41. Obayya, M.; Maashi, M.S.; Nemri, N.; Mohsen, H.; Motwakel, A.; Osman, A.E.; Alneil, A.A.; Alsaied, M.I. Hyperparameter Optimizer with Deep Learning-Based Decision-Support Systems for Histopathological Breast Cancer Diagnosis. *Cancers* **2023**, *15*, 885. [[CrossRef](#)] [[PubMed](#)]

**Disclaimer/Publisher's Note:** The statements, opinions and data contained in all publications are solely those of the individual author(s) and contributor(s) and not of MDPI and/or the editor(s). MDPI and/or the editor(s) disclaim responsibility for any injury to people or property resulting from any ideas, methods, instructions or products referred to in the content.